Oxidation behaviour of stainless steel–Al coatings produced by co-sputtering and reactive sputtering

Kun He [a], Hao Gong [a,*], Kaiyang Zeng [b], Zhengwei Li [c], Wei Gao [c]

[a] *Department of Materials Science, The National University of Singapore, 10 Kent Ridge Crescent, Singapore 119260, Singapore*
[b] *Institute of Materials Research and Engineering, Singapore, Singapore*
[c] *Department of Chemical and Materials Engineering, The University of Auckland, Auckland, New Zealand*

Abstract

Unbalanced magnetron sputter deposition (UMSD) was employed to produce thin alloy coatings for high temperature application. The coatings consist of 310S stainless steel and Al. Two methods have been used to deposit the coatings. One is the conventional co-sputtering with 310S steel and Al targets in argon, and the other is co-sputtering with oxygen introduced into the system, in which a part of Al was oxidised to alumina. SEM and XRD results showed different microstructures of the coatings obtained by using these two methods, resulting in different oxidation behaviour. While these two coatings formed protective oxide scales during oxidation, breakaway oxidation took place on the uncoated stainless steel samples. © 2000 Elsevier Science B.V. All rights reserved.

Keywords: Co-sputtering; Reactive sputtering; 310S stainless steel; Coatings; Oxidation

1. Introduction

Magnetron sputter deposition is one of the most important techniques to produce thin films for electronic materials and device applications. It was also used to produce coatings for improving wear, corrosion resistance and other surface properties [1]. Unbalanced magnetron sputter deposition (UMSD) is a further development of the conventional magnetron sputtering to overcome the problem of low deposition rate [2]. Recently, UMSD has been applied to produce overlay coatings for high temperature applications [3–6]. The oxidation resistance can be greatly improved by these types of coatings.

Stainless steels are the most common materials used in many industries, including applications at high temperatures with oxidising/corrosive environments. Under such working conditions, protective oxide scales are essential for reliable service. Al oxides and Cr oxides are chemically stable and mechanically strong, possessing very good protective ability at high temperatures. The aim of this study is to produce mixed alloy and alloy-oxide coatings that

* Corresponding author. Tel.: +65-874-6598; fax: +65-7763-604.

E-mail address: masgongh@nus.edu.sg (H. Gong).

can form protective oxides on the surface, therefore to improve the oxidation resistance of stainless steels.

2. Experimental

Specimens of stainless steels AISI 310 and 304, with dimensions of $15 \times 10 \times 3$ mm and $10 \times 10 \times 0.3$ mm, respectively, were polished with 3-μm diamond paste and then cleaned ultrasonically in acetone. Their chemical compositions are listed in Table 1. 310S steel and Al (99.99% Al, Superconductor Materials) were used as targets. To further clean and enhance the film's adhesion to the substrates, the substrates were cleaned by argon glow discharge via reverse sputtering before deposition process. The targets were also cleaned with 20-min sputtering while the shutter was closed.

Coatings were produced using the radio frequency magnetron sputtering system established at the National University of Singapore. During the deposition process, the stage on which the substrates were placed was rotated at 15 rpm. This process guarantees the physical and chemical uniformity of the coatings, and also ensures that each edge of the sample is coated. High purity argon was introduced into the chamber. The working pressure in the chamber was controlled at 20 mTorr for all experiments. During reactive sputtering, oxygen was introduced into the chamber. The partial pressure of oxygen was 0.8 mTorr. To achieve a higher adhesion between the substrate and film, the concept of "gradient coatings" was used. The whole deposition process was divided into three stages. In the first stage, radio frequency power of 300 W was applied to the stainless steel target to deposit a thin layer of stainless steel on the stainless steel substrate surface. In the second stage, a smaller proportional RF power of 7% total output energy was introduced to the Al target. In the final stage (the longest stage), the power on Al

Table 1
Chemical analysis of the alloy samples (wt.%)

Alloy	Cr	Ni	Mn	Si	Fe
310S	25.7	19.2	1.3	0.51	Bal.
304	18.2	8.5	1.1	0.60	Bal.

Table 2
Deposition processes

Runs	Stage 1: 1.5 h	Stage 2: 1.5 h	Stage 3: 4 h
G1: co-deposition	310S	310S + 7% Al	310S + 14% Al
G2: reaction-deposition	310S	310S + 7% Al, 0.8 mTorr O_2	310S + 14% Al, 0.8 mTorr O_2

was increased to 14% of the total output. The coating processes are summarised in Table 2. The thickness of the coatings deposited on the substrates was measured to be in the range of 2.5–3.0 μm.

Oxidation experiments were conducted using a DuPont Thermogravimetric Analyser (TGA). The samples were placed in a platinum basket, which was put into the TGA furnace and heated to the desired temperature rapidly. Airflow was then introduced into the furnace, and the samples were oxidised at 900°C for 5 h.

A PHILIPS FEG scanning electron microscope (HRSEM) was used to study the detailed morphology of the coatings and the oxidised samples. X-ray diffraction (XRD) with Cu Kα radiation was used to identify the phase structure. Nano-indentation tests were conducted by UMIS-2000H nano-indentation machine, which is set up in Institute of Materials Research and Engineering (IMRE), Singapore.

3. Results and discussions

3.1. Coating microstructures

Fig. 1a and b is the SEM images showing the morphologies of the coatings produced by co-deposition (G1) and reactive deposition (G2), respectively. The chemical compositions of coatings G1 and G2 were determined by EDX, and shown in Table 3.

As shown in Fig. 1, coating G1 consists of particles with an average size of 200 nm, each of which may consist of a few smaller grains or sub-grains. Particles with light contrast are dispersed randomly over the coatings. EDX analysis indicated that these light-contrast particles have ~ 4 wt.% Al, higher than the average of 2.5% in the coatings. In coating
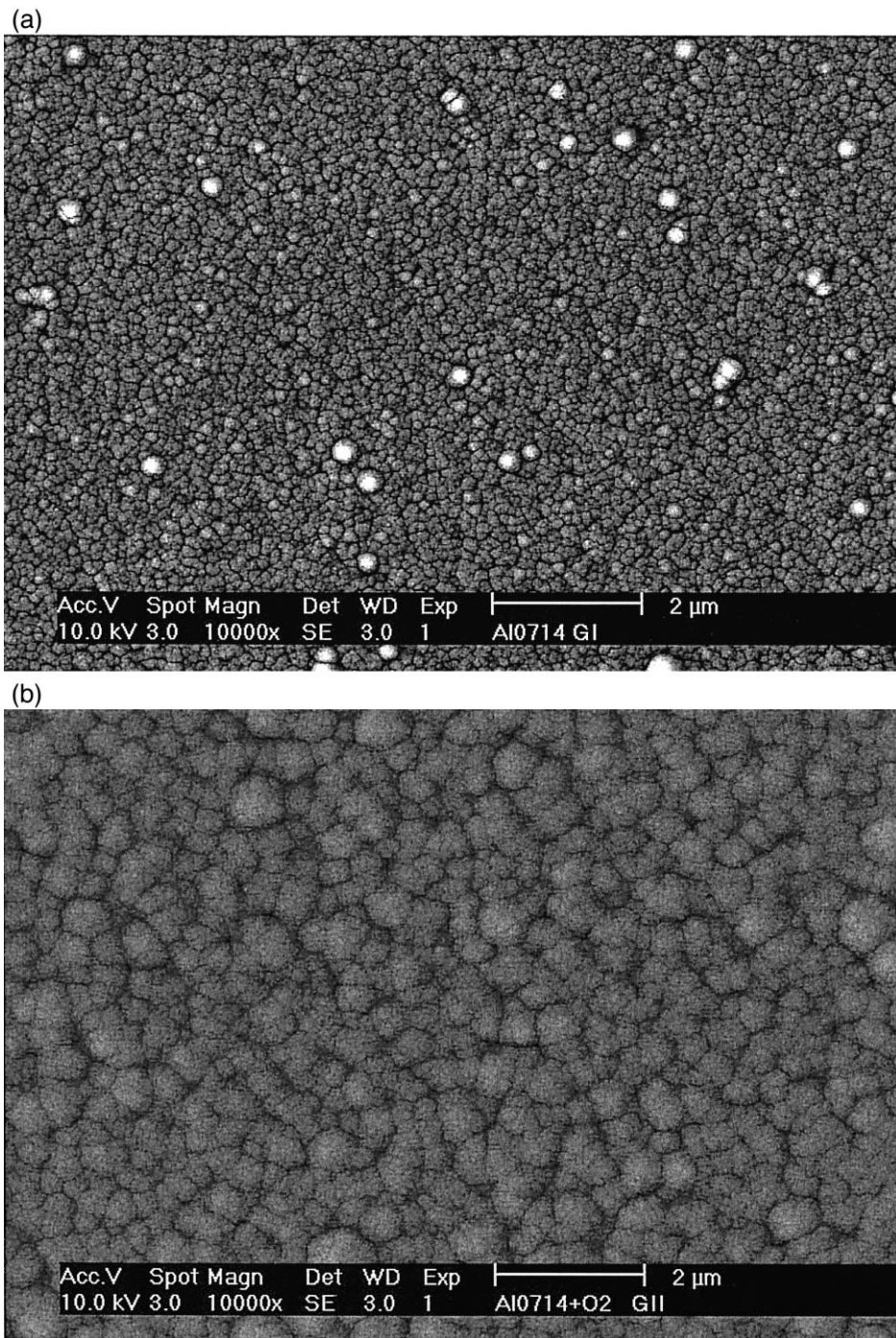
Fig. 1. SEM surface morphologies of the coatings produced by (a) co-deposition (G1) and (b) reactive deposition (G2).

G2, the clusters were larger (~ 500 nm) than in coating G1 and packed more closely together, show-ing a uniform microstructure. The clusters do not show sharp crystal features, but each of them ap-

Table 3
Chemical compositions of the coatings (wt. % / at. %)

Coating	Processing	O	Al	Si	Cr	Fe	Ni
G1	Co-deposition	7.0/20.0	2.5/4.2	0.4/0.7	24.7/21.9	47.2/38.9	18.2/14.3
G2	Reactive co-deposition	24.2/51.1	3.4/4.5	0.5/0.6	18.9/12.3	37.5/22.7	15.5/8.9

peared to consist of many small grains or sub-grains. The XRD spectra showed in Fig. 2 indicate that coating G1 had mainly $\gamma(111)$ diffraction, evidence of preferred (111) orientation. The XRD pattern from coating G2 showed no clear peaks, indicating poor crystallinity with very small grain size or amorphous structure.

3.2. Nano-indentation tests of the coatings

Hardness and elastic modulus of standard stainless steel 310 and coatings G1 and G2 were tested by a UMIS-2000H Nano-indentation machine, with a maximum load of 10 mN. Twenty-five indents were made on each sample surface. The measured hardness and elastic modulus of samples (before oxidation) were listed in Table 4.

These results indicated that G2 coating has the highest hardness, followed by coating G1 and 310S steel. This can be explained as coating G2 contains dispersive oxides and showed a dense microstructure, Fig. 1b. Coating G2 also has a relatively high elastic modulus. On the other hand, coating G1 has an increased hardness compared with 310S steel but slightly decreased elastic modulus, perhaps because of the Al content. The hardness is a microstructure

Fig. 2. X-ray diffraction patterns of 304 stainless steel, G1 and G2 coatings.

sensitive property while Young's modulus is microstructure insensitive.

3.3. Oxidation kinetics

Fig. 3 plots the oxidation kinetic curves obtained with TGA, which shows that the oxidation of uncoated samples followed a linear rate law at the initial stage:

$$Y = K_1 t + C \tag{1}$$

where Y is the mass gain of unit area, K_1 is the linear rate constant, t is the exposure time and C is a constant. After about 3-h oxidation, the reaction rate increased dramatically, an evidence of the breakaway oxidation [7], indicating poor oxidation resistance.

The oxidation of coating G1 followed a parabolic rate law:

$$Y^2 = K_p t + C \tag{2}$$

with a parabolic rate constant K_p, indicating a diffusion controlled reaction kinetics [7,8].

The oxidation of G2 samples seems to follow an approximately logarithmic rate law:

$$Y = K_{\log} \log(t + t_0) + A \tag{3}$$

representing a reaction with a high initial rate, which dropped down rapidly to a low level when a protective film formed on the surface. It should be noted that the above rate laws were calculated from a relatively short oxidation time because of the thin
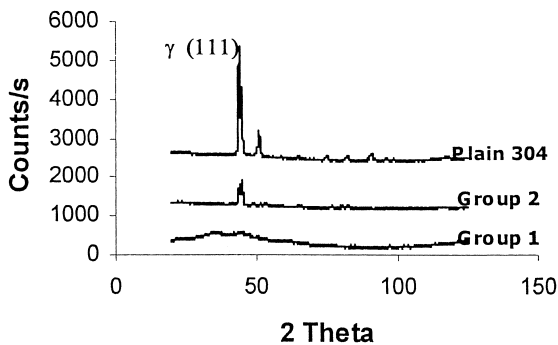
Table 4
Results of nano-indentation tests for 310 stainless steel and coatings

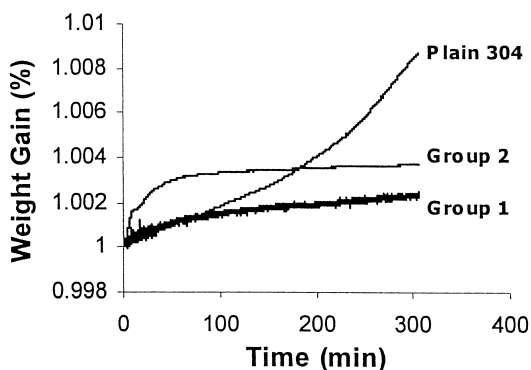| Sample	310S	G1	G2
Hardness (GPa)	4.15	5.11	6.24
E (GPa)	120.7	112.7	166.6
Equivalent Vickers hardness (HV)	381	469	573

Fig. 3. Oxidation kinetic curves of 304, G1 and G2 samples oxidized at 900°C in dry airflow.

coating layers. Thick coatings are being prepared for longer time oxidation tests.

The initial oxidation rate of coating G2 was high compare to that of coating G1. After ∼ 60 min, however, the kinetic curve became almost flat with little further mass gain. This may be explained by the formation of a protective oxide scale. The fast oxidation rate at the initial stage is believed to be affected by the fine crystal grain structure that contains a high density of grain boundaries as the "short-circuit" diffusion paths. These diffusion paths promote selective oxidation of Al [6], forming Al oxide scales with good protective ability. Another reason of the high initial oxidation rate is the rough surface of coating G2, which provides a large reaction area at the initial stage of oxidation. The kinetic curve plotted in Fig. 3 was calculated using the geometric surface area, which may be substantially smaller than the reaction surface area. The reaction area decreases with the formation of the protective oxide scale, reducing the mass gains as shown in Fig. 3. The grain boundaries can also provide "pinning" sites that improve the spallation resistance of the oxide scale.

3.4. Oxide morphology

SEM morphologies of the oxide scales formed on the uncoated 304 steel, G1 and G2 coated samples were quite different (Fig. 4). The oxide grains formed on the surface of the uncoated 304 steel varied over a wide range in size (from 0.7 to 4 μm). The large

polyhedral crystals are believed to be the product of the breakaway oxidation with the structure of Fe–Cr spinel phase [9]. This type of oxide does not have good protective ability, and its growth rate is high. The oxides formed on coating G1 showed a much smaller and uniform grain size (∼ 0.28 μm) compared to the uncoated samples. They also appeared to be more compact. EDS analysis showed that the oxides formed on coating G1 contain a small amount of Al and more Cr compared to the oxides formed on 304 steel, although the basic composition of the oxides is similar. No breakaway oxidation products can be seen. The oxide scale formed on coating G2 was also uniform and compact. The morphology of the oxides was, however, different from that of coating G1 even though the grain size was similar. Two different types of grains can be seen in Fig. 4c: the underneath round-shaped large grains (∼ 0.5 μm) and the top fine grains (∼ 0.2 μm). The top grains were mostly formed on the grain boundary areas of the round-shaped grains, implying a formation mechanism due to grain boundary diffusion. The accurate composition of the oxides formed on coating G2 was difficult to determine due to the thin layer, but EDS analysis also indicated a relatively high Cr and a small amount of Al.

In general, the microstructures of these three group samples agreed with the oxidation kinetics described above. In contrast to the uncoated samples, both coatings G1 and G2 showed protective oxidation kinetics, and no scale spallation was observed.

3.5. Nano-indentation tests of the oxidized coatings

The results of nano-hardness test of the coating surface after oxidation were shown in Table 5.

The surface hardness and elastic modulus measured by the nano-indentation machine were again different for the uncoated steel and two coatings, indicating the surface oxides formed during oxidation are different. The oxides formed on the coatings have a higher hardness and Young's modulus, perhaps due to the stronger, more compact nature of the oxide layers. There is very little information on the nano-hardness testing of the as-formed oxide scales. As this technique may be useful for studying the properties of surface oxide layers, more work is
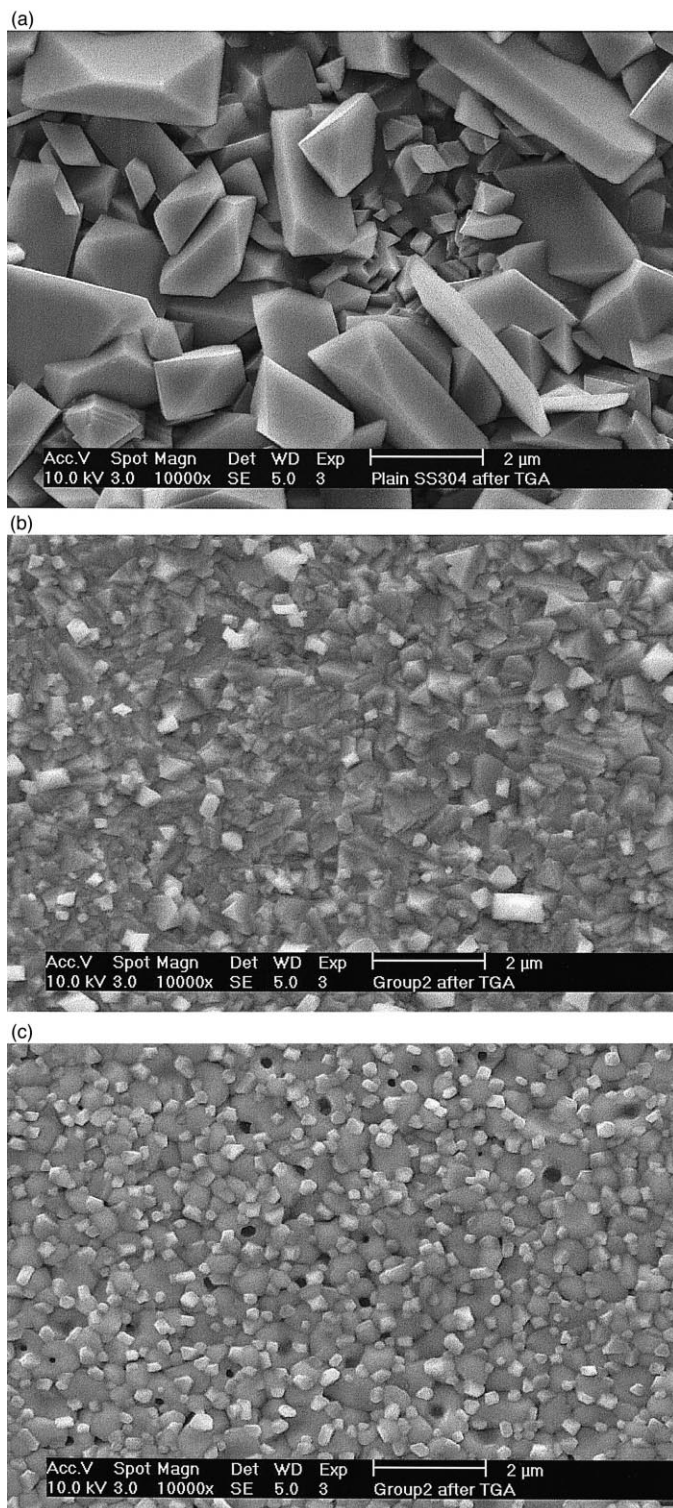
Fig. 4. SEM morphologies showing the oxides formed on (a) uncoated 304, (b) G1 coating, and (c) G2 coating after oxidation at 900°C for 5 h.

Table 5
Results of nano-indentation tests of the oxide layers formed on 310S and coatings

Sample	310S	G1	G2
Hardness (GPa)	1.62	3.21	4.55
E (GPa)	32.2	47.1	68.2
Equivalent Vickers hardness (HV)	149	295	418

being conducted to understand the results obtained from nano-indentation tests.

4. Conclusions

Co-sputtering and reactive sputtering deposition were used to produce mixture coatings of 310S stainless steel and Al. The coatings deposited by the different techniques have different microstructures. The coatings produced by co-sputtering showed a strong preferred $(111)\gamma$ orientation, while the coatings produced with reactive co-sputtering exhibited a poor crystallinity. Protective oxide layers were formed on these coatings during high temperature oxidation. The oxidation kinetics changed from the non-protective, breakaway type for the un-coated steel to the protective, parabolic or logarithmic type for the coatings. The microstructures of the oxide layers formed on the uncoated steels and the coatings were also different, generally in agreement with the observed oxidation kinetics. Nano-indentation tests indicated different mechanical properties for the sample surfaces before and after oxidation.

References

[1] W.-D. Munz, Surface and Coatings Technology 48 (1995) 81.
[2] B. Window, N. Savvides, Journal of Vacuum Science and Technology, A 4 (1986) 453.
[3] S. Zhu, Surface and Coatings Technology 71 (1997) 9.
[4] Z. Liu, W. Gao, K. Dahm, Y. He, High Temperature Materials and Processes 16 (1997) 159.
[5] Z. Liu, W. Gao, K. Dahm, F. Wang, Oxidation of Metals 50 (1998) 51.
[6] Z. Liu, W. Gao, K. Dahm, F. Wang, Acta Materialia 46 (1998) 1691.
[7] P. Kofstad, High Temperature Corrosion1988, p. 259, New York.
[8] P Kofstad, High Temperature Corrosion1988, p. 18, New York.
[9] F.H. Stott, F.I. Wei, Materials Science and Technology 5 (1989) 1140.